Modeling Techniques for Magnetostrictive Actuators

Ralph C. Smith [1]
Department of Mathematics
Iowa State University
Ames, IA 50011

Abstract

Techniques for modeling hysteresis and material nonlinearities in magnetostrictive materials are presented. Hysteresis in these materials is due to both the driving magnetic field and stress relations within the material and is significant throughout most of the drive range of the material. Two characterizations are presented here. The first model is posed in terms of Preisach operators and is purely phenomenological in nature. The second model is physics-based with parameters related to measurable properties of the input magnetic field. The two approaches are illustrated in the context of an Euler-Bernoulli beam model which incorporates magnetostrictive actuators.

Keywords: Magnetomechanical model, magnetostrictive materials, Preisach model, Terfenol

1. Introduction

New and promising control transducers are currently being designed using magnetostrictive materials. These materials exhibit the dual properties that strains are generated in response to an applied magnetic field while conversely, material stresses in the materials produce domain changes which yield measurable magnetic effects. In certain rare earth materials such as Terfenol-D, these effects are sufficiently large to warrant the material's use as control actuators and sensors. The forces generated by magnetostrictive transducers can be of the order of forces generated by large and more massive magnetic shakers, and are significantly larger than those produced by electrostrictives or piezoceramics. Due to their capacity for generating large strains and forces, magnetostrictive actuators have been employed as ultrasonic transducers, sonar projectors and actuators for controlling vibrations in thick structures and heavy industrial machinery. To fully utilize their capabilities as either sensors or actuators, however, the hysteresis and nonlinearities inherent to the magnetostrictive materials must be characterized in a manner amenable to parameter estimation and control applications.

Two techniques for characterizing hysteresis in magnetostrictive materials are presented here. The first model is formulated in terms of generalized Preisach or Krasnoselskii-Pokrovskii operators. This provides a phenomenological or empirical characterization of the input/output relations of the magnetostrictive materials which circumvents unmodeled or unknown physical mechanisms. The advantage of this technique lies in its generality. The model requires the estimation of a large number of nonphysical parameters, however, and does not provide physical insights into the material dynamics. The second model is formulated through consideration of reversible and irreversible domain wall movements in the material. Hence it is physics-based with parameters related to magnetic characteristics of the input magnetic field. This characterization is obtained through extension of the ferromagnetic hysteresis models of Jiles and Atherton [8, 9, 10] to magnetostrictive actuators. The two approaches are illustrated in the context of an Euler-Bernoulli beam model which incorporates magnetostrictive actuators.

The configuration of magnetostrictive transducers and physical properties of the magnetostrictive materials are described in Section 2. The source and form of the nonlinearities and hysteresis are detailed to illustrate issues to be addressed in the models. A phenomenological model based upon Preisach or Krasnoselskii-Pokrovskii operators is discussed in Section 3 and the physics-based model is presented in Section 4. The two approaches are illustrated in the context of an Euler-Bernoulli beam model in Section 5.

[1] Email – rsmith@iastate.edu; URL – http://www.math.iastate.edu/rsmith

2. Magnetostrictive Transducers

Issues which must be addressed when modeling magnetostrictive materials are illustrated in the context of the transducer depicted in Figure 1. This transducer is typical of those currently employed in applications and contains the basic components required for experimental use as a control actuator. Details regarding the construction and performance of this transducer can be found in [6].

The primary components of the transducer consist of a magnetostrictive rod, a wound wire solenoid, and a cylindrical permanent magnet. In current transducers, the magnetostrictive material is typically composed of terbium and dysprosium alloyed with iron. A commonly employed material is Terfenol-D (Ter: terbium, fe: iron, nol: Naval Ordinance Laboratory, D: dysprosium) which is constructed as a cylindrical rod and placed in the center of the transducer. The sensor/actuator capabilities of the material are provided by magnetic domains which rotate in the presence of an applied magnetic field. As depicted in Figure 2a, the domains are primarily oriented perpendicular to the longitudinal rod in the absence of an applied field. Prestressing the rod with the spring washer serves to increase the number of domains perpendicular to the axis (see Figure 2b) and place the material in compression. This latter objective is necessary due to the inherent brittleness of Terfenol-D. In the presence of a magnetic filed, the domains rotate so as to align with the field. Consequently, if the field is applied in the direction of the rod axis, the domains rotate in the sense depicted in Figure 2c and significant strains are generated. This is termed the Joule effect and provides the actuator capabilities of the transducer. Sensing is accomplished through the measurement of the magnetic fields which result when mechanical stresses cause rotations of the domains (Villari effect). Details regarding these effects can be found in [7, 14] while further discussion regarding the physics of magnetic domains is given in Section 4.

The strains generated through an applied field are always positive since rotation of the domains from the pre-stressed perpendicular state leads to an increase in the rod length. As indicated in Figure 3, the relationship between the applied magnetic flux or induction B and strain ϵ is also highly nonlinear with saturation occurring at large field strengths. Moreover, slight hysteresis also exists between B and ϵ at high drive levels [12] (this is not depicted in the figure).

The generation of bidirectional strains is accomplished through either a DC current I_0 applied to the solenoid which surrounds the rod or an enclosing cylindrical permanent magnet which provides a biasing magnetic induction B_0. A time varying current $I(t)$ is then used to vary the induction in the rod between 0 and B_m. This provides the capability of generating both positive and negative strains.

To model the transducer for actuator and sensor purposes, it is necessary to characterize the relationship between the current I applied to the solenoid, the resulting magnetic field H, the associated magnetization M, and finally, the generated strains ϵ. Furthermore, the quantification must incorporate the contributions due to the permanent magnet.

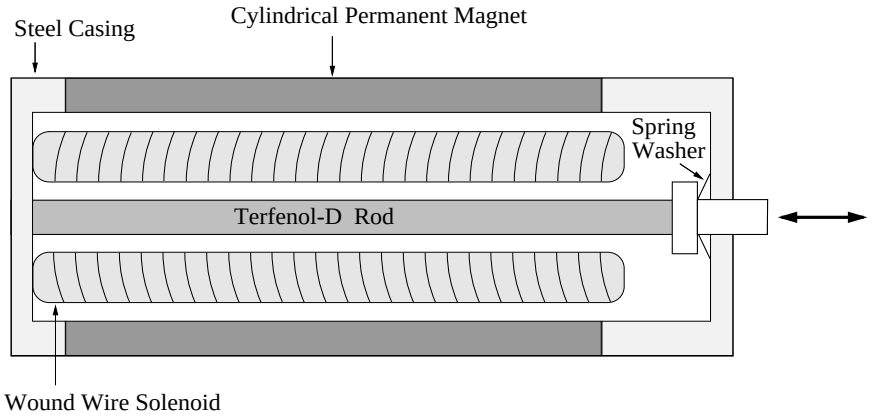

Figure 1. Cross section of a typical Terfenol-D magnetostrictive transducer.

The magnetic induction and field are related by the permeability μ which is defined as

$$\mu = \frac{B}{H}$$

(see [7] for the general relations between H, M and B). The magnetic field is due both to the solenoid and the permanent magnet. The magnetic induction from the permanent magnet is approximated by $B = \mu H_0$ while Ampère's law yields $B = \mu n I$, where n is the number of turns per unit length in the solenoid, as the approximate magnetic induction due to the solenoid (this relation neglects edge effects, air gaps, et cetera).

For Terfenol-D, the permeability μ is highly nonlinear and exhibits significant hysteresis as indicated by the induction/field relations depicted in Figure 4a. To indicate the stress dependence, the permeability in magnetostrictive applications is often denoted by μ^σ. The hysteretic relationship between the magnetic field, magnetic induction and material stress are then inherently manifested in the field-strain relations as shown in Figure 4b.

Furthermore, the nonlinear relationship between the applied current and resulting strains is augmented by constitutive nonlinearities in the magnetostrictive materials. For example, experimental results in [3, 5] indicate that the Young's modulus E^H for Terfenol is dependent upon the applied magnetic field which partially accounts for the dependence of magnetic hysteresis on the material stress. Furthermore, these experiments demonstrate that other material properties including magnetomechanical coupling coefficients are highly sensitive to operating conditions such as prestress level, AC drive levels, operating frequencies and temperature. This indicates some of the requirements for the Preisach and magnetomechanical models described in subsequent sections.

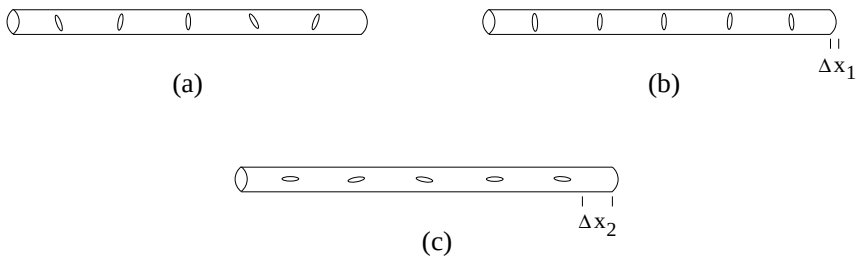

Figure 2. Magnetic domains in the Terfenol-D rod; (a) Orientation of domains in unstressed rod in absence of applied magnetic field; (b) Orientation of domains in prestressed rod with no applied field; (c) Orientation of domains in prestressed rod when field is applied in direction of longitudinal rod axis.

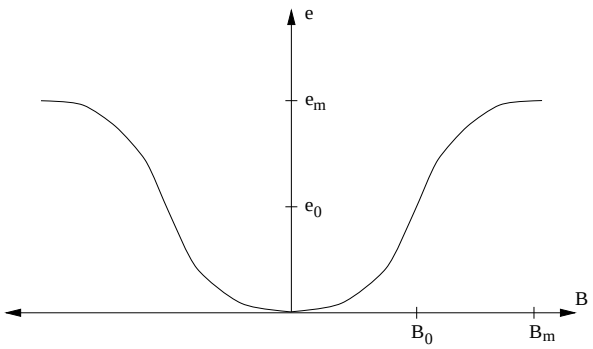

Figure 3. Strain distribution e generated by an applied magnetic induction B.

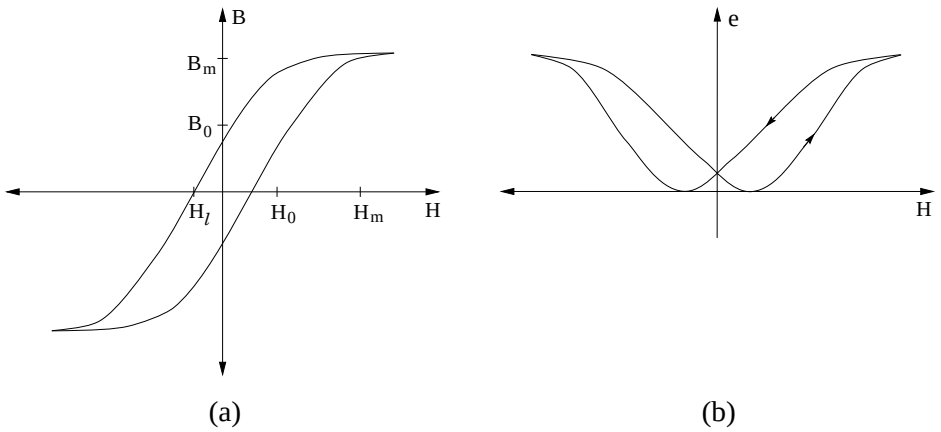

Figure 4. (a) Relationship between the magnetic field strength H and the magnetic induction B. (b) Applied magnetic field H and resulting strain distribution e.

3. Preisach Models

A model based on Preisach or Krasnoselskii-Pokrovskii operators is discussed here. This section summarizes material in [13], which in turn depends upon theory from [1], and the reader is referred to those references for further details.

To motivate the general kernels, we first illustrate with a single delayed, relay operator $\hat{k}$. This kernel is characterized in terms of crossing times $\tau(t)$ defined by

$$\tau(t) = \{\eta \in (0,T] \,|\, u(\eta) = s_1 \text{ or } u(\eta) = s_2\}$$

where $s = (s_1, s_2)$ are points in the Preisach half plane

$$\mathcal{S} = \left\{ s \in \mathbb{R}^2 \,|\, s = (s_1, s_2), s_1 < s_2 \right\}$$

and u denotes an input function. The values s_1, s_2 are threshold values for the multivalued kernel as reflected in the definition

$$[\hat{k}_s(u,\xi)](t) = \begin{cases} [\hat{k}_s(u,\xi)](0) & \text{if} \quad \tau(t) = \emptyset \\ -1 & \text{if} \quad \tau(t) \neq \emptyset \text{ and } u(\max \tau(t)) = s_1 \\ +1 & \text{if} \quad \tau(t) \neq \emptyset \text{ and } u(\max \tau(t)) = s_2 \,. \end{cases}$$

A depiction of this kernel is given in Figure 5a. The starting value

$$[\hat{k}_s(u,\xi)](0) = \begin{cases} -1 & \text{if} \quad u(0) \leq s_1 \\ \xi & \text{if} \quad s_1 < u(0) < s_2 \\ +1 & \text{if} \quad u(0) \geq s_2 \end{cases}$$

defines the initial state of the kernel in terms of the parameter $\xi \in \{-1, 1\}$.

The output remains on a branch until a threshold is reached in the monotonically increasing input u. At that point, the output jumps to the other saturation value and remains there until the other threshold value is reached. For example, an output response starting with a value of -1 will retain that value until $u(t)$ reaches s_2. The output then jumps to $+1$ until the threshold value of s_1 is reached.

The classical Preisach operators are then defined in terms of parallel collections of these single relay operators. To this end, we let $\mathcal{M}$ denote the set of all finite, signed Borel measures on $\mathcal{S}$ and let f be a Borel measurable function mapping $\mathcal{S} \to \{-1, 1\}$. For $u \in C[0,T]$ and $\nu \in \mathcal{M}$, the Preisach operator is defined by

$$[\hat{P}_\nu(u,f)](t) = \int_{\mathcal{S}} [\hat{k}_s(u, f(s))](t) d\nu(s).$$

The goal in the parameter identification problem is to estimate ν so that a model response "fits" experimental data in a least squares sense.

While this provides an operator which is useful for many applications, this classical definition does not yield a kernel, and hence operator, which is continuous with respect to either time or parameters. Specifically, as proven in [1], the mapping in time

$$t \mapsto [\hat{k}_s(u,\xi)](t)$$

and the parameter space mapping

$$s \mapsto [\hat{k}_s(u,\xi)](t)$$

are discontinuous for the classical Preisach kernel $\hat{k}_s(u,\xi)$. Continuity in time is important from a physical perspective while continuous parameter dependence is crucial for the development of practical parameter estimation methods.

To avoid the difficulties associated with the discontinuous mappings, a Krasnoselskii-Pokrovskii kernel of the type discussed in [1] is employed. This kernel is somewhat less general than the influence operators considered in [11] and arises as an extension of smoothed Preisach operators. These operators differ from the previously-defined Preisach operator in the manner through which an envelop of admissible paths is defined. In this case, an envelop is provided by translates

$$r_{s_1} = r(x - s_1)$$
$$r_{s_2} = r(x - s_2)$$

of a Lipschitz continuous ridge function $r(x)$ as depicted in Figure 5b. For monotone inputs $u_m \in C[0,T]$, a monotone output operator is defined by

$$[\mathcal{R}(u_m,\xi)](t) = \begin{cases} \max\{\xi, r(u_m(t) - s_2)\} & \text{if } u_m \text{ is non-decreasing} \\ \min\{\xi, r(u_m(t) - s_1)\} & \text{if } u_m \text{ is non-increasing}\,. \end{cases}$$

In terms of this operator, a kernel is defined for piecewise monotone inputs $u_{pm} \in C[0,T] \cap S_{1,j}[0,T]$, $S_{1,j}[0,T]$ is the set of piecewise linear splines with j knots in $[0,T]$, in the following manner. The initial value of the operator is taken to be $\mathcal{R}_0 \in \xi$. A kernel k_s is then defined recursively on each subinterval by

$$[k_s(u_{pm},\xi)](t) = [\mathcal{R}(u_{pm},\mathcal{R}_{k-1})](t)\ ,\ t \in [t_{k-1},t_k] \tag{1}$$

where $\mathcal{R}_k \equiv \mathcal{R}(u_{pm},\mathcal{R}_{k-1})(t_k)\ ,\ k = 1,\cdots,j$. The input and action of this kernel are illustrated in Figure 6. This provides a definition of the kernel useful for computational algorithms in which inputs are discretized in terms of a piecewise linear basis. This definition is readily extended to arbitrary $u \in C[0,T]$ through standard density arguments as detailed in [11]. Details illustrating the use of this kernel for characterizing hysteresis in magnetostrictive actuators are provided in Section 5.2.

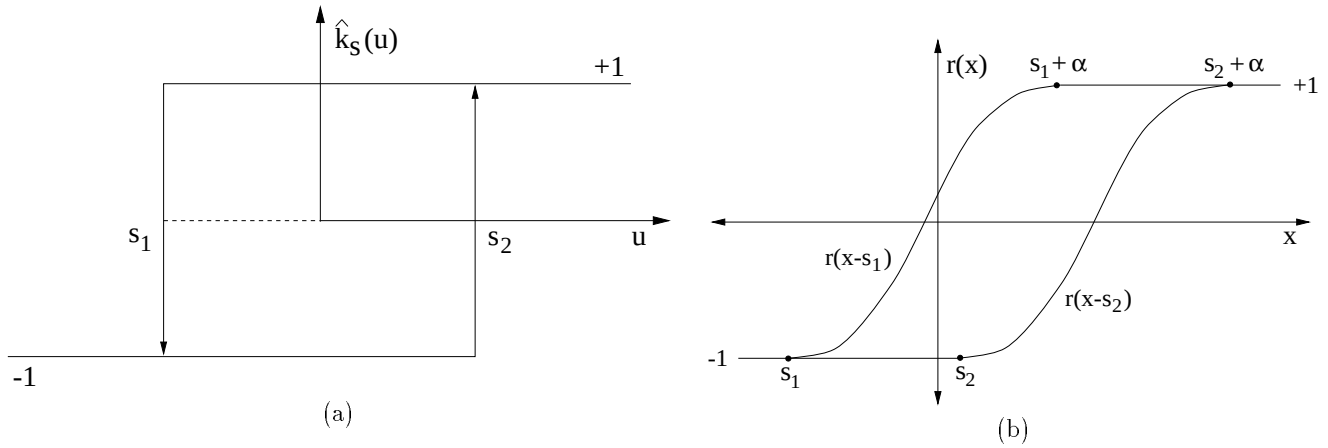

Figure 5. (a) Single Preisach relay operator with threshold values s_1, s_2. (b) Hysteresis envelop provided by the translates r_1 and r_2 of the ridge function $r(x)$.

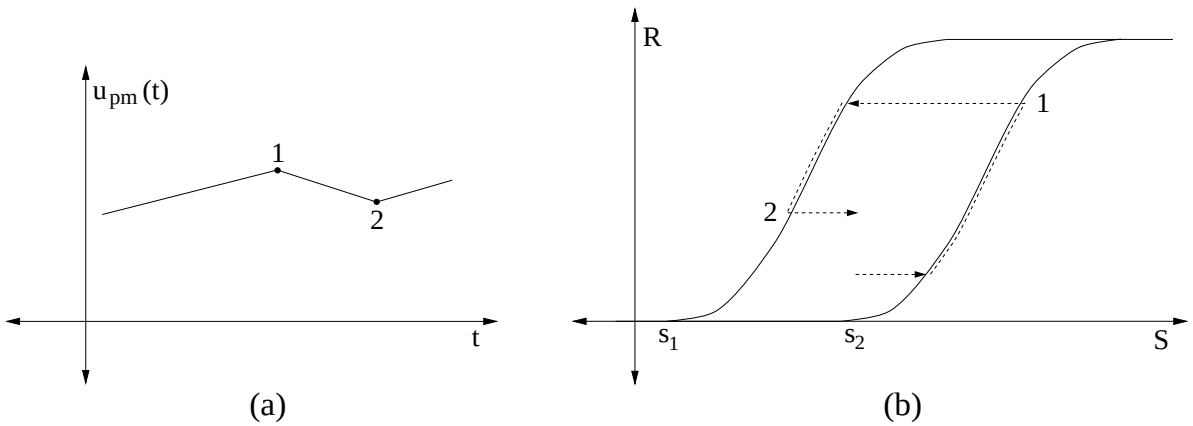

Figure 6. (a) Piecewise monotone input. (b) Output from the Krasnoselskii-Pokrovskii kernel in response to a piecewise monotone input.

4. Domain Wall Model

The physics-based model considered here is based upon the theory that magnetization in ferromagnetic materials is due to the realignment of domains, which are defined as regions in which magnetic moments are always aligned, in response to an applied magnetic field. From energy considerations, it has been established that the primary reorientation of magnetic moments occurs within transition layers, or domain walls, between the domains. For a material which is free from defects, bending and translation of domain walls leads to anhysteretic (hysteresis free) behavior which is completely reversible. Most materials, however, contain defects (e.g., carbides in steel or second phase materials such as the rare earth rich phase in Terfenol) which impede domain wall motion due to the reduction in energy which occurs when the wall intersects the defect. At low magnetic field levels, the walls remain pinned or close to the defect and the motion is reversible. The motion becomes irreversible at higher energy levels due to wall intersections with remote defects or pinning sites. This leads to the hysteresis observed in ferromagnetics. It should be noted that the presence of such domains has been verified experimentally while domain wall effects are manifested through phenomena such as the Barkhausen discontinuities observed in magnetization curves.

The property to be quantified is the strain which results when the magnetostrictive material is subjected to an applied magnetic field. A reasonable measure of this strain is the magnetostriction $\lambda \equiv \frac{d\ell}{\ell}$ which indicates the relative change in length of the material from the ordered but unaligned state to the state in which domains are aligned. While the magnetostriction does not quantify DC effects or the effects of domain order, it does quantify the strains generated in a Terfenol actuator.

An important issue when modeling magnetostrictive materials such as Terfenol concerns the form of material and magnetic anisotropies. In the absence of applied stresses, cubic anisotropy models are often assumed with the saturation magnetostriction λ_s defined in terms of the independent saturation magnetostrictions λ_{100} and λ_{111} in the $\langle 100 \rangle$ and $\langle 111 \rangle$ directions, respectively. As detailed in [7], under the assumption that the material contains a large number of domains and has no preferred grain orientation, averaging of domain effects yields the expression

$$\lambda_s = \frac{2}{5}\lambda_{100} + \frac{3}{5}\lambda_{111}$$

for the total saturation magnetostriction (typical saturation values for Terfenol are $\lambda_{100} = 90 \times 10^{-6}$ and $\lambda_{111} = 1600 \times 10^{-6}$).

As depicted in Figure 2b, the application of a longitudinal compressive stress to a Terfenol rod has the effect of aligning the domain moments perpendicular to the rod axis. Application of a magnetic field in the direction of the rod axis then causes domain rotations which, to first approximation, yield the magnetostriction

$$\lambda = \frac{3}{2}\frac{\lambda_s}{M_s^2}M^2 \,. \tag{2}$$

Here M_s and M denote the saturation and applied magnetic fields, respectively. Note that this expression ignores higher order contributions to the magnetostriction (see [8]) and magnetostrictive hysteresis (see [12]). Issues regarding these latter contributions in magnetostrictive actuators are currently under investigation.

To characterize the magnetization M for typical actuator/sensor applications, it is necessary to quantify the anhysteretic magnetization M_{an}, the reversible magnetization M_{rev} and the irreversible magnetization M_{irr} in terms of the applied magnetic field and exogenous stresses. In general, the magnetization is dependent upon the crystal anisotropy of the material. If sufficiently large prestresses are applied to the material, however, stress anisotropy will dominate the crystal anisotropy.

In this case, the effective magnetic field is given by

$$H_{eff} = H + \alpha M + H_\sigma$$

where αM quantifies contributions due to the magnetic interaction between domains and H_σ is the field resulting from magnetoelastic domain interactions. From thermodynamic considerations, the effective field component due to an applied stress σ can be shown to be

$$H_\sigma = \frac{3}{2}\frac{\sigma}{\mu_0}\left(\frac{\partial \lambda}{\partial M}\right)_T$$

where λ again denotes the bulk magnetostriction, μ_0 is the free space permeability, and the subscript T denotes constant temperature (see [8, 12] for details). Note that with the approximation (2) for λ, the effective field can be expressed as

$$H_{eff} = H + \alpha M + \frac{9}{2}\frac{\lambda_s \sigma}{\mu_0 M_s^2} M.$$

Under the assumption of constant domain density N, the anhysteretic magnetization is then defined in terms of the Langevin function

$$\begin{aligned} M_{an}(H,\sigma) &= M_s \mathcal{L}(H_{eff}/a) \\ &\equiv M_s \left[\coth\left(\frac{H + \alpha M + (9\lambda_s\sigma/2\mu_0 M_s^2)M}{a}\right) - \left(\frac{a}{H + \alpha M + (9\lambda_s\sigma/2\mu_0 M_s^2)M}\right)\right]. \end{aligned} \tag{3}$$

The constant a is theoretically given by $a = Nk_BT/\mu_0 M_s$ where k_BT represents the Boltzmann or thermal energy. In applications, this parameter can be determined from physical properties of the experimental hysteresis curve through the algorithm of [10]. We reiterate that this expression for the anhysteretic magnetization is derived under the assumption that magnetic anisotropies dominate crystal anisotropy effects and is valid for applications in which materials are sufficiently prestressed. For applications in which prestresses are small, the Langevin equation (3) is no longer valid since different anisotropic energy is measured in different directions. For that case, the contributions of magnetic moments must be individually summed to obtain the anhysteretic magnetization.

The expression (3) for the anhysteretic magnetization incorporates the rotation of domain moments but does not include the dissipative effects of domain wall motion. The inclusion of domain wall bowing yields an additional reversible magnetization component M_{rev} while translation of domains and intersection with remote pinning sites contributes an irreversible magnetization component M_{irr}.

As detailed in [8], consideration of energy dissipation due to pinning and unpinning yields the expression

$$\frac{dM_{irr}}{dH} = \frac{M_{an} - M_{irr}}{\frac{k\delta}{\mu_0} - \left(\alpha + \frac{3}{2}\frac{\sigma}{\mu_0}\left(\frac{\partial^2 \lambda}{\partial M^2}\right)_T\right)(M_{an} - M_{irr})} \tag{4}$$

for the differential susceptibility of the irreversible magnetization (the pinning constant k and sign parameter δ can be estimated from the experimental hysteresis curve). The reversible magnetization quantifies the degree to which domain walls bulge before breaking loose from pinning sites, and to first approximation is given by

$$M_{rev} = c(M_{an} - M_{irr}) \tag{5}$$

(see [9] for details concerning this derivation). The constant c is the ratio of the initial and anhysteretic differential susceptibilities. Finally, the total magnetization is given by

$$M = M_{rev} + M_{irr}\ . \tag{6}$$

Hence for materials in which uniaxial stress anisotropies dominate the inherent crystal anisotropies, the total stress-dependent magnetization can be computed through combination of (4), (5) and (6) with the anhysteretic magnetization given by (3).

For drive levels below the saturation magnetization, a first approximation to the strain generated by the actuator is provided by (2). It should be noted that this expression includes the magnetoelastic effects due to stress through the inclusion of these effects in the anhysteretic magnetization. As detailed in the next section, this provides a mechanism for including the effects of prestress and elastic stresses when computing actuator inputs in structural applications utilizing magnetostrictive transducers.

5. Thin Beam Actuator Model

To illustrate the use of the Preisach and magnetomechanical frameworks described in the last two sections to characterize hysteresis in magnetostrictive materials, we consider the modeling of magnetostrictive actuators mounted to a cantilever beam as depicted in Figure 7. The actuators are considered to be mounted to the clamps at the fixed edge of the beam so that mass loading from the actuators themselves is minimized. A rigid bar is used connect the end of the Terfenol rod in the transducer to the beam. By driving the transducers out-of-phase, bending moments are generated in a manner which can be used to attenuate beam vibrations. As described by [4], this experimental setup has been used in initial experiments to determine the potential of magnetostrictive transducers as structural actuators. Due to limitations in models and control laws, driving currents in the experiments were restricted to a range in which linearized results could be employed. Even in this restricted regime, the results of [4] demonstrate the utility of the magnetostrictive transducers. An advantage of magnetostrictive actuators over piezoceramics and electrostrives in many structural applications is due to the magnitude of the forces generated by the magnetostrictives. Hence they can produce effective bending moments in applications where other actuators will quite often fail.

For modeling purposes, we take the beam to have length ℓ, width b and thickness h with the transverse displacement denoted by w. The density, Young's modulus, Kelvin-Voigt damping coefficient and air damping coefficient for the beam are denoted by ρ_b, E_b, c_{D_b} and γ, respectively. The cross-sectional area of the Terfenol rod is denoted by A_{mag} while the Young's modulus for the Terfenol rod is denoted by E^H. The length and width of the connecting bar are denoted by ℓ_r and b_r, respectively, while the bar density is given by ρ_r.

The Euler-Bernoulli equation

$$\rho(x)\frac{\partial^2 w}{\partial t^2}(t,x) + \gamma\frac{\partial w}{\partial t}(t,x) + \frac{\partial^2 \mathcal{M}_{int}}{\partial x^2}(t,x) = f(t,x) + \frac{\partial^2 \mathcal{M}_{mag}}{\partial x^2}(t,x)$$

$$\left.\begin{aligned} w(t,0) = \frac{\partial w}{\partial x}(t,0) = 0 \\ \mathcal{M}_{int}(t,\ell) = \frac{\partial \mathcal{M}_{int}}{\partial x}(t,\ell) = 0 \end{aligned}\right\} \quad , \quad t > 0 \tag{7}$$

with appropriate initial conditions is used to model the beam dynamics. Exogenous surface forces to the beam are denoted by $f(t,x)$ while $\rho(x)$ is the composite density for the structure. The internal and external bending moments are denoted by $\mathcal{M}_{int}$ and $\mathcal{M}_{mag}$, respectively.

Figure 7. Cantilever beam with magnetostrictive actuators.

To determine appropriate functional forms for the density and internal moments, the structural contributions due to the connecting bar and Terfenol rod must be quantified. We assume here that the connecting bars are perfectly rigid and contribute mass to the beam but do not affect the bending moments (we neglect air resistance to the bars). The actuator and Terfenol rod are considered to be supported from the boundary clamps so they do not contribute mass to the beam. The Terfenol is assumed to contribute an elastic stress which is taken to be uniform across the cross-sectional area of the rod. Finally, it is assumed that the Terfenol rod is subjected to a prestress σ_0 by the spring washer (see Figure 1).

Under the assumption of uniform cross-sectional strains in the magnetostrictive rods, the elastic stress in an individual rod is approximated in terms of the elastic strain $\tilde{\epsilon}$ by

$$\begin{aligned} \tilde{\sigma} &= E^H \tilde{\epsilon} \\ &\approx E^H \left(h/2 + \ell_r\right) \frac{\partial^2 w}{\partial x^2} . \end{aligned} \tag{8}$$

The density, stiffness and Kelvin-Voigt damping parameters for the structure are then taken to be

$$\begin{aligned} \rho(x) &= \rho_b hb + 2\rho_r b_r \ell_r \chi_{rod}(x) \\ EI(x) &= \frac{E_b h^3 b}{12} + 2A_{mag} E^H \left(h/2 + \ell_r\right)^2 \chi_{rod}(x) \\ c_D I &= \frac{c_{D_b} h^3 b}{12} \end{aligned} \tag{9}$$

where the location of the rods is delineated by the characteristic function χ_{rod} which has a value of 1 in the region covered by the connection bar and is 0 elsewhere. We have assumed here that material damping in the Terfenol rod is negligible; if desired, Kelvin-Voigt damping in the rod can be incorporated through an obvious modification of the parameter $c_D I$. The internal moment is then given by

$$\mathcal{M}_{int}(t,x) = EI(x)\frac{\partial^2 w}{\partial x^2}(t,x) + c_D I \frac{\partial^3 w}{\partial x^2 \partial t}(t,x) .$$

It should be noted that the passive or internal contributions due to the connecting bars and magnetostrictive actuator are dependent upon the exact experimental setup and different assumptions and models may also be used incorporate these contributions. In all cases, the parameters $\rho, EI, c_D I$ and γ must be estimated through a least squares fit to experimental data to attain a reasonable model for the specific experimental device. While the values determined by (9) can be used as initial values for optimization routines, they cannot be used with certainty when modeling the experimental apparatus due to inaccuracies in manufacturer specifications, et cetera.

5.1. External Moments – Domain Wall Model

We consider here a characterization of the external moment $\mathcal{M}_{mag}$ in terms of the domain wall model discussed in Section 4. To attain bidirectional strains, we will assume that an offset DC current I_0 is used to bias the input current to each actuator. Ampère's law then yields the magnetic field

$$H(t) = n[I(t) + I_0]$$

where again, n is the number of terms per unit length in the solenoid and $I(t)$ is the time-dependent current applied to the solenoid. For systems in which elastic stresses are reversible, it follows from (5) and (6) that the total stress-dependent magnetization which results from the magnetic field is given by

$$M(\sigma,t) = cM_{an}(\sigma,t) + (1-c)M_{irr}(\sigma,t) \tag{10}$$

where M_{irr} is determined by (4). The applied stresses

$$\begin{aligned} \sigma(t) &= \sigma_0 + \tilde{\sigma}(t) \\ &= \sigma_0 + E^H \left(h/2 + \ell_r\right) \frac{\partial^2 w}{\partial x^2}(t) \end{aligned}$$

in (10) reflect both the prestress σ_0 and the internal elastic stress (8). The total stress for the magnetostrictive material in an individual actuator is then given by

$$\sigma_{tot}(t) = E^H[\tilde{e}(t) - \lambda(t)]$$

where the bulk magnetostriction λ generated by the magnetization (10) is given by (2). The mechanical stress $\tilde{\sigma} = E^H\tilde{e}$ has already been included in the internal moment through (9). The external moment generated by the pair of Terfenol rods is then given by

$$\mathcal{M}_{mag}(t,x) = 2A_{mag}E^H\left(h/2 + \ell_r\right)^2\lambda(t)\chi_{rod}(x)\,.$$

When employed in the Euler-Bernoulli equation (7), this provides a physics-based characterization of the Terfenol actuator inputs to the thin beam model. This characterization is fully coupled in the sense that reversible magnetomechanical effects due to stresses are included in the generating magnetization and resulting moments. For time-dependent elastic stresses which are sufficiently large so as to be irreversible, energy mechanisms of the type discussed in [8] can be employed to incorporate magnetomechanical effects.

5.2. External Moments – Preisach Model

The Preisach approach provides a purely mathematical characterization for the generated moment through the fitting of the hysteresis and material nonlinearities in terms of the kernels described in Section 3. Specifically, the external moment generated by the magnetostrictive transducer is taken to be

$$\mathcal{M}_{mag}(t,x) = 2A_{mag}\left(h/2 + \ell_r\right)[P_\nu(I,\xi)](t)\chi_{rod}(x)$$

where

$$[P_\nu(I,\xi)](t) \equiv \int_{\mathcal{S}}[k_s(I,\xi)](t)\,d\nu(s)\,.$$

The kernel k_s is the extension of that defined in (1) to input currents $I \in C[0,T]$. For a given set of experimental operating conditions, the measure ν must be estimated through a fit to experimental data. This then yields a characterization of the external moment which can be utilized in actuator or controller design. It should be noted that the advantage to this approach lies in its generality. It requires a large number of parameters, however, and does not directly utilize knowledge of the material physics.

6. Conclusions

Two techniques for characterizing hysteresis in magnetostrictive actuators were presented here. The first model, formulated in terms of Preisach kernels, provides a phenomenological characterization of hysteresis and material nonlinearities. The advantage of this approach lies in its applicability in situations involving physical mechanisms which are unmodeled or poorly understood. The resulting model requires the estimation of a large number of nonphysical parameters, however, and does not provide physical insights into the material dynamics. The second model is physics-based with parameters related to magnetic characteristics of the input magnetic field. Through thermodynamic considerations and incorporation of magnetomechanical effects, the influence of stress on actuator dynamics is directly included in this model whereas these effects are only indirectly included in the Preisach model. Comparison of these models for an experimental system is currently under investigation and will be reported in a future work.

Acknowledgements

The author expresses sincere appreciation to H.T. Banks, F.T. Calkins and D.C. Jiles for input regarding the modeling techniques employed here. This research was supported in part by the National Aeronautics and Space Administration under NASA Contract Number NAS1-19480 while the author was a visiting scientist at the Institute for Computer Applications in Science and Engineering (ICASE), NASA Langley Research Center, Hampton, VA 23681. Additional support was also provided by NASA grant NAG-1-1600.

References

[1] H.T. Banks, A.J. Kurdilla and G. Webb, "Identification of hysteretic control influence operators representing smart actuators; Part I: formulation," CRSC Technical Report CRSC-TR96-14, April, 1996; *Mathematical Problems in Engineering*, submitted.

[2] H.T. Banks, R.C. Smith and Y. Wang, *Smart Material Structures: Modeling, Estimation and Control*, Masson/John Wiley, Paris/Chichester, 1996.

[3] F.T. Calkins and A.B. Flatau, "Transducer based measurement of Terfenol-D material properties," Proceedings of the SPIE Conference on Smart Structures and Integrated Systems, Paper No. 67, Vol. 2717, February 1996.

[4] F.T. Calkins, R.L. Zrostlik and A.B. Flatau, "Terfenol-D vibration control of a rotating shaft," Proceedings of the 1994 ASME International Mechanical Engineering Congress and Exposition, Chicago IL; In *Adaptive Structures and Composite Materials Analysis and Applications* AD-Vol. 45, pp. 267-274, 1996.

[5] M.J. Dapino, F.T. Calkins, D.L. Hall and A.B. Flatau, "Measured Terfenol-D material properties under varied operating conditions," Proceedings of the SPIE Conference on Smart Structures and Integrated Systems, Paper No. 66, Vol. 2717, February 1996.

[6] D.L. Hall and A.B. Flatau, "Nonlinearities, harmonics and trends in dynamic applications of Terfenol-D," Proceedings of the SPIE Conference on Smart Structures and Intelligent Materials, Vol. 1917, Part 2, pp. 929-939, 1993.

[7] D.C. Jiles, *Introduction to Magnetism and Magnetic Materials*, Chapman and Hall, New York, 1991.

[8] D.C. Jiles, "Theory of the magnetomechanical effect," *Journal of Physics D: Applied Physics*, 28, pp. 1537-1546, 1995.

[9] D.C. Jiles and D.L. Atherton, "Theory of ferromagnetic hysteresis," *Journal of Magnetism and Magnetic Materials*, 61, pp. 48-60, 1986.

[10] D.C. Jiles, J.B. Thoelke and M.K. Devine, "Numerical determination of hysteresis parameters for the modeling of magnetic properties using the theory of ferromagnetic hysteresis," *IEEE Transactions on Magnetics*, 28(1), pp. 27-35, 1992.

[11] M. Krasnoselskii and A. Pokrovskii, *Systems with Hysteresis*, Springer, Berlin, 1989; Russian Edition, Nauka, Moscow, 1983.

[12] M.J. Sablik and D.C. Jiles, "Coupled magnetoelastic theory of magnetic and magnetostrictive hysteresis," *IEEE Transactions on Magnetics*, 29(3), pp. 2113-2123, 1993.

[13] R.C. Smith, "Hysteresis modeling in magnetostrictive materials via Preisach operators," *Journal of Mathematical Systems, Estimation and Control*, submitted.

[14] E. du Trémolet de Lacheisserie, *Magnetostriction: Theory and Applications of Magnetoelasticity*, CRS Press, Ann Arbor, 1993.